POLARIMETRIC AZIMUTHAL SPECTRAL HISTOGRAM EXPOSES TYPES OF MIXED SCATTERERS AND THE CAUSE FOR UNEXPECTED POLARIMETRIC AVERAGES

Svetlana Bachmann [1, 2, 3], *Dusan Zrnic* [1], *Victor DeBrunner* [4]

[1] – National Severe Storm Laboratory, Norman, OK
[2] – Cooperative Institute for Mesoscale Meteorological Studies,
[3] – The University of Oklahoma,
[4] – Florida State University

ABSTRACT

Echoes detected by polarimetric weather radar in clear air contain signals from air and biological scatterers. Discriminating the various scatterer types from a composite echo is challenging due to variability in scatterres' quantity, azimuthal dependences of their polarimetric properties, and uneven mixing in resolution volumes. We use polarimetric spectral densities to estimate the volume content by constructing two dimensional (2D) histograms. The dimensions used to form image are Doppler velocity and polarimetric variable. The assimilation of these histograms in azimuth results in a 3D-azimuthal-spectral-histogram (3DASH). This representation allows us to use transparency for small occurrences to visualize the 3D-signatures of dominant content. The scatterer types have distinguishable signatures in 3DASH due to their diverse physical shapes, scattering properties, different headings, and speeds. 3DASH can help to understand what constitutes the polarimetric averages of the resolution volume. 3DASH can help provide resources for establishing intrinsic polarimetric values/functions for different types of biological scatterers, which are necessary for scatterer classification algorithms.

Index Terms— pulse Doppler radar, radar polarimetry, spectral domain analysis, scattering parameters measurement

1. INTRODUCTION

During bird and insect migration seasons, the weather radar displays (velocity, reflectivity, and polarimetric variables) depict values which represent neither wind nor biological scatterers' signatures. Recovering the wind or retrieving the birds' signatures are both challenging tasks for the following reasons: 1) Polarimetric values vary in azimuth due to body shapes and orientation of biological scatterers [5], [6], [7], [9]; 2) The uneven mixing of different scatterer types (i.e., insects and birds) in the same resolution volumes and varying altitudes of flight in the same resolution volume create additional difficulties in discrimination [1], [9].

Radar signal processing proceeds in range and sample time to produce radials of data. A radial consists of echoes collected at approximately the same azimuthal location by transmitting several pulses and detecting the returned echoes. Operational weather radars (NEXRAD) transmit 17 pulses to determine the reflectivity and 64 pulses for the Doppler velocity computation. The latter is sufficient for spectral analyses. Spectral analyses in weather radar applications refers to both the process of estimating the power spectral density for any resolution volume and of enhancing the signal by de-noising and clutter filtering in the frequency domain [2]. Improved radar moments (reflectivity, velocity, etc.) can be estimated from the filtered power spectral densities. Clutter filtering schemes can eliminate radar returns that have a known band of frequencies (i.e. frequencies corresponding to zero velocity returns such as ground clutter) or returns with a recognized and estimated frequency location (i.e. strong point return from an airplane). However, conventional spectral analyses methods are inadequate where the resolution volumes contain mixed biological scatterers. Furthermore, while spectral analyses can reveal multimodal content of a resolution volume, the analysis will conflate peaks caused by useful signals with those caused by clutter. Polarimetric spectral analyses have demonstrated potential to deal with such situations [1]. We provide a brief review of polarimetric spectral densities in Section 2.

Now, suppose that biological scatterers are uniformly distributed over the scanned region. Then their polarimetric returns would appear symmetric relative to the scatterers' left-to-right body axis, and non-symmetric with respect to the front-to-back axis due to physical body proportions. Further, suppose there is another type of biological scatterers with different body proportions in the same region. The symmetry is expected to be distorted when the two types are flying with different headings. Moreover, the polarimetric variables computed for a resolution volume of such a region are composites of the polarimetric values of the two types. Therefore, general scatterer classification algorithms combine birds and insects in the same group called "biological scatterers." Although many investigators

report that insects have larger values of differential reflectivity than birds, there are azimuthal locations where this difference is minimal [9]. Moreover, such discrimination applies only if there is dominance of one type over the other. The azimuthal dependence of the polarimetric variables, the unknown number of scattering types and their relative dominance make discrimination difficult. We present a novel approach for investigating the intrinsic (not mean) polarimetric values and their azimuthal dependence in Section 3. The illustrative examples are in Section 4. A full understanding of the polarimetric composite is an important stage for interpreting the resolution volume average values which are commonly used in scatterers classification algorithms.

2. POLARIMETRIC SPECTRAL DENSITIES

This section reviews the computation of polarimetric spectral densities and describes ways to enhance viewing of the spectra by separating the signals from noise and artifacts.

2.1. Spectral densities of polarimetric variables

Conventionally in weather radar, the power spectral density (PSD) is estimated from the time series data optionally weighted with a window. We use Von Hann window. For the weather radar with dual polarization there are two PSDs for each resolution volume. The polarimetric spectral densities are estimated from the spectral coefficients of the two PSDs [1], [4], [8]. The spectral densities of differential reflectivity are computed according to

$$Z_{DR}(k) = 10\log_{10}\frac{|s_h(k)|^2}{|s_v(k)|^2} + C, \text{(dB)}, \qquad (1)$$

where M is the number of pulses or spectral coefficients for a resolution volume; k is an ordered number that takes values from 1 to M and can be translated to radial velocity in the unambiguous interval from $-v_a$ to v_a; $s_h(k)$ and $s_v(k)$ are complex spectral coefficients of the H and V signals; and C is the calibration constant. The spectral densities of copolar correlation are estimated from a running 3-point average on contiguous complex spectral H-V pairs

$$\rho_{hv}(k) = \frac{\sum_{m=<k-1>_M}^{<k+1>_M} s_h(m)s_v{}^*(m)}{\sqrt{\sum_{m=<k-1>_M}^{<k+1>_M}|s_h(m)|^2 \sum_{m=<k-1>_M}^{<k+1>_M}|s_v(m)|^2}} \qquad (2)$$

by taking its absolute value. The spectral density of the differential phase is the argument of complex value estimated in equation (2) with subtracted system phase. The polarimetric variables obtained with standard processing techniques are equivalent to averages of intrinsic polarimetric spectral densities.

2.2. Spectral density enhancement

The procedure for subtracting the noise power from the power spectral densities is well established [2]. The question that remains is how to determine the noise level. We estimate the noise level for each range location using rank order statistics on spectral coefficients and computing the mean of the lowest half of spectral coefficients. We use 128 pulses for spectral analyses. We have examined spectral densities prior to choosing this noise estimation scheme and noticed visual enhancement of coherent features.

Polarimetric spectral densities can be enhanced by the simultaneous censoring of those spectral coefficients whose copolar correlation coefficient is below 0.7, or power is below some nominal or estimated noise level.

3. 3D HISTOGRAM FORMATION

The polarimetric spectral densities are used to compute a 2D histogram as a function of the Doppler velocity and the polarimetric variable. The 2D histogram is computed for a chosen volume of the scan. The volume can include multiple adjacent range locations and/or several neighboring radials. For a radar scan with a 250 meter range spacing and one degree spacing in azimuth, there are four spectra for each kilometer. The histogram image will most likely depict the clustering of spectral coefficients with similar properties as an increasing number of spectra are included in the analyses. For example, a range span of 5 km consists of 20 spectra, and a range span of 20 km has 80 spectra. Unfortunately a large range span covers different altitudes and is a suspect to other unfavorable effects such as significant beam broadening at farther ranges. Therefore a span in azimuth might be considered. Consider that a volume that is 5 km by 3 degrees contains 60 spectra that can be used for analyses. When the chosen volumes are established, the polarimetric spectral densities (Section 2) are estimated and the 2D histograms are computed. An explanatory example is provided in Fig.1. Fig.1a shows a possible spectral density field while Fig.1b depicts the histogram of that field. The images of such 2D histograms are collected in azimuth as shown in Fig.2a. The resultant box of occurrences (Fig.2b) is the 3D azimuthal spectral histogram, abbreviated 3DASH. Small occurrences obscure the interior of the 3DASH. Setting transparency for the small occurrences allows us to expose the interior of the cube and to observe the clustered signature and irregularities [3], [10]. The transparency permits to us to look inside the 3DASH and observe properties that are otherwise hidden (Fig.2c). The degree of transparency can be adjusted. Rotation and slicing can be used to view the signature and to evaluate the intrinsic values of the polarimetric variables and their dependencies.

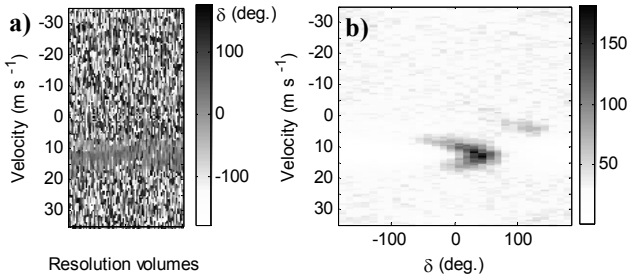

Fig.1. Explanatory example: (a) polarimetric spectral densities of a chosen volume (here, backscatter differential phase) and (b) resulting 2D histogram

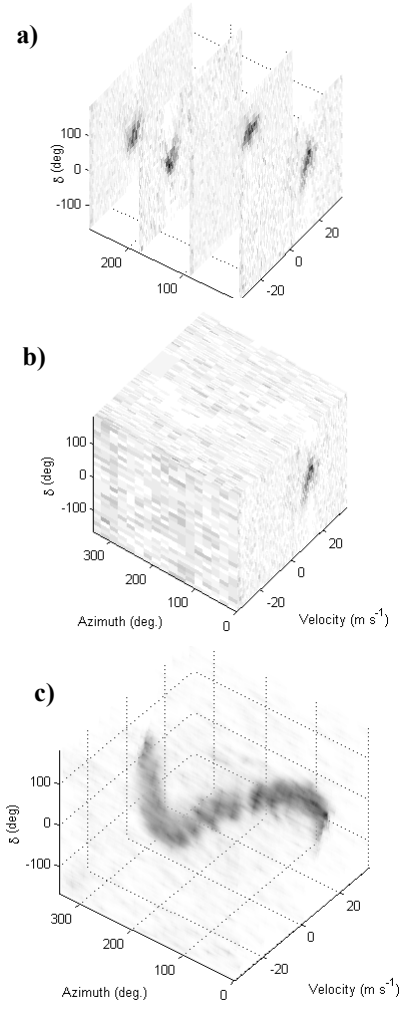

Fig.2. 3DASH formation from 2D histograms: (a) five slices with 2D histograms, (b) cube of 2D histograms in all azimuth locations, (c) transparency for small occurrences allows to look inside the cube.

4. EXAMPLES

To demonstrate the utility of 3DASH in the evaluation of the intrinsic polarimetric values and their azimuthal dependencies, we present examples of clear air returns during bird migration. This case occurred on September 7, 2004 at radar location 4UT. Returns from migrating birds and wind-borne insects were detected over a large region. Judicious spectral analyses of these data indicated that birds and insects shared space (up to about 70 km in range or approximately below 1.5 km in altitude), had about 10 m s^{-1} difference in mean velocities, and about 30° difference in heading [1]. Polarimetric spectral analyses also indicated that large portions of the bird returns average out if both the censoring (Section 2.2) and range averaging methods are applied. This is due to the sporadic nature of the birds' presence in any of the resolution volumes.

For demonstration purposes we evaluate the 2D histograms for relatively large regions, 20° in azimuth and 20 km in range. The range is chosen in the "mid range" interval from 30 km to 50 km to insure sufficient signal to noise ratio and the absence of ground clutter residuals. The 3DASH of differential reflectivity, of copolar correlation coefficients and of the differential phase are shown in Figure 3a, 3b, and 3c, respectively. There are 18 azimuthal locations, 128 bins for the radial velocity with values from -35 to 35 m s^{-1} and 30 bins for the polarimetric values.

In the 3DASH of differential reflectivity (Fig.3a) clusters form two broad curls. One of these shapes is a relatively better formed helix. The shape indicates smaller velocities and larger differential reflectivity values and therefore is indicative of insects. The other clustering appears irregular and is indicative of birds. Rotation of the 3DASH will aid a user to fully appreciate the capability of this novel display. Fig.3a shows a view (a position of the 3D object) in which the helix-like shape from insects and the other shape of sporadic occurrences from birds are displaced from each other in velocity and direction.

In the 3DASH of copolar correlation (Fig.3b) clusters form a sinusoid-like curl (in the azimuth velocity plane) of high correlation values, indicating small insects. The other occurrences with gradually diminishing values from high – and certainly overlapping the insect signature – to small are from birds. An unexpected observation is a burst of high correlation values at 200° with high velocity values caused by birds. This region can be also observed in Z_{DR}. This is a case wherein birds have higher Z_{DR} and ρ_{hv} than insects.

A possible explanation is a favorable orientation. This is an important observation. Previously reported comparisons of the mean Z_{DR} values of insects and birds still hold. Nonetheless, it is important to realize that there are situations in which the bird and insect mean Z_{DR} signatures can be misinterpreted.

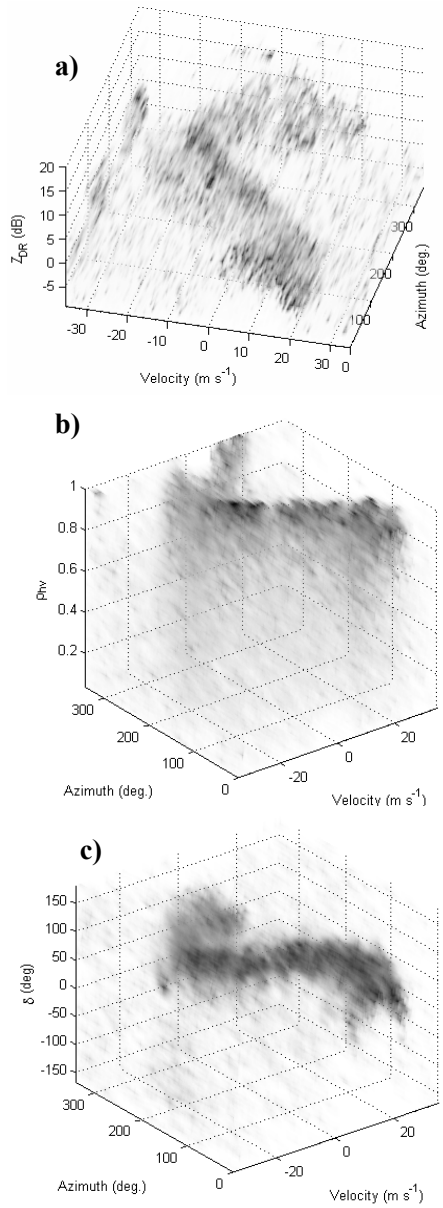

Fig.3. 3DASH examples (a) differential reflectivity, (b) copolar correlation coefficient; (c) differential phase.

The 3DASH of differential phase (Fig.3c) clusters form a helix-like curl which projects a sinusoidal path in the velocity-azimuth-plain. The scatterers moving in unison and exhibiting similar shape and orientation are expected to produce a well-defined helix as seen in Fig. 3c. Birds have noise-like differential phases. Insects have a narrow band of phases that change in azimuth. Therefore this 3DASH depicts the insects well. This is by far the most visually pleasing 3DASH.

5. CONCLUSIONS

We presented 3DASH as a visualization tool for estimating and exploring the values of intrinsic polarimetric densities of scatterers and their azimuthal dependencies. The polarimetric variables obtained with standard processing techniques are equivalent to the averages of intrinsic polarimetric spectral densities. The 3DASH can reveal the cause of unexpected polarimetric values in signatures of atmospheric scatterers. We demonstrated the potential of 3DASH to expose locations with exceptional values (outliers) in a case where the polarimetric signatures of birds and insects could easily be confused if one were trying to determine scatterer type by using only the polarimetric averages. The 3DASH can be used to explore all contributing scatterer signatures or only dominant scatterers if censoring is applied.

6. REFERENCES

[1] S. M. Bachmann and D. S. Zrnic, "Spectral Density of Polarimetric Variables Separates Biological Scatterers in the VAD Display," *J. Atmos. and Ocean. Technol.*, in print 2007.

[2] R. J. Doviak and D.S. Zrinc, *Doppler Radar and Weather Observations*, Academic Press, 1985.

[3] J. D. Foley, A. van Dam, S. K. Feiner, and J. F. Hughes, *Computer* Graphics*: Principles and Practice*, Addison-Wesley Publishing Company, Inc., 1996.

[4] V. Kezys, E. Torlaschi, and S. Haykin, "Potential capabilities of coherent dual polarization X-band radar," *26th Int. Conf. on Radar Meteorology*, Norman, OK, Amer. Meteor. Soc., pp. 106-108, 1993.

[5] R. P. Larkin and R. H. Diehl, "Spectrum width of birds and insects on pulsed Doppler radar," *IEEE Trans. on Geoscience and Remote Sensing*, 2003.

[6] T. Schuur, A. V. Ryzhkov, and P. Heinselman, "Observation and classification of echoes with the polarimetric WSR-88D Radar," NSSL Lab., Norman , OK, *Tech. Rep*., Oct. 2003.

[7] J. W. Wilson, T. M. Weckwerth, J. Vivekanandan, R. M. Wakimoto, and R. W. Russell, "Boundary layer clear air radar echoes: Origin of echoes and accuracy of derived winds," *J. Atmos. Ocean. Tech*.., vol. 11, pp. 1184–1206, 1994.

[8] F. J. Yanovsky, H. W. J. Russchenberg, and C. M. H. Unal, "Retrieval of information about turbulence in rain by using Doppler-polarimetric Radar," *IEEE Trans. Microw. Theory Tech*., vol. 53, pp. 444–450, 2005.

[9] D. S. Zrnić and A. V. Ryzhkov, "Observation of Insects and Birds with Polarimetric Radar," *IEEE Trans. Geosci. Remote Sens*., vol. 36, pp. 661–668, 1998.

[10] Mathworks, 2006: *MATLAB Technical manual*. Function Reference. Available: http://www.mathworks.com.